

# Second-Order Acceleration Models for an MMAE Target Tracker

BARBARA J. WHEATON

PETER S. MAYBECK, Fellow, IEEE  
Wright-Patterson AFB

The performance of a multiple model adaptive estimator (MMAE) for an enhanced correlator/forward-looking-infrared tracker for airborne targets is analyzed in order to improve its performance. Performance evaluation is based on elemental filter selection and MMAE estimation error sizes and trends. The elemental filters are based on either first or second-order acceleration models. Improved filter selection is achieved by using acceleration models that separate the frequency content of acceleration power spectral densities into non-overlapping regions with second-order models versus the more traditional overlapping regions with first-order models. A revised tuning method is presented. The maximum a posteriori (MAP) versus the Bayesian MMAE is investigated. The calculation of the hypothesis probability calculation is altered to see how performance is affected. The impact of the ad hoc selection of a lower bound on the elemental filter probability calculation to prevent filter lockout is evaluated. Parameter space discretization is investigated.

## I. INTRODUCTION

A multiple model adaptive estimator (MMAE) is composed of a parallel bank of elemental Kalman filters, each based on a different assumed system parameter or model. The observed properties of the residuals from each elemental filter are then used to evaluate the probability that the assumed model of each filter best represents the current real-world situation [8]. The purpose of this work is to discuss the enhancement of the ability of the MMAE to select the most appropriate elemental filter as system dynamics vary. The MMAE used in this investigation is one developed for the forward-looking infrared (FLIR)/correlator tracker that can be used in a high energy laser weapon system [10, 11, 17, 18]. The investigation focuses on two areas: the selection of the models to use in the elemental filters of the tracking filter and the altering of the algorithm the MMAE uses to make its estimate.

The tracking of airborne targets is currently accomplished for this application with a conventional correlator. This correlator tracker has several limitations contributing to tracking errors. Two important ones are as follows.

- 1) There is a time lag due to the time it takes the correlator algorithm to correlate the current frame of FLIR outputs to the previous frame and for the actual pointing gimbals to point the FLIR sensor in the next appropriate direction to keep the target in the center of the field of view (FOV). The FOV is the number of pixels the correlator and, later, the Kalman filter (KF) uses in estimating target position. The FLIR sensor is 300-by-500 pixels. Normally, 8-by-8 pixels is the maximum sized tracking "window" used in the algorithm.

- 2) Apparent target motion results from physical phenomena like atmospheric jitter and bending and vibration of the tracker optics. The correlator does not distinguish true target motion from this erroneous apparent motion.

A KF is added to the tracker to overcome these limitations.

An "enhanced" correlator tracker is used so the dynamics of the target can be modeled as linear and the target shape need not be known [15]. The correlator algorithm compares the current FLIR image with a template instead of the image from the previous time frame. The template estimates the target shape by averaging the centered image over the previous 10 time frames. The "measurement" given to the KF is the offset of the image from the center of the FOV, as produced by the enhanced correlator. The resulting linear KF reduces computational loading and gives comparable performance to an extended KF that

Manuscript received March 16, 1992; revised October 8, 1993.

IEEE Log No. T-AES/31/1/08006.

Authors' address: B. J. Wheaton, WL/AAAI, Wright-Patterson Air Force Base, OH 45433-6583; P. S. Maybeck, Air Force Institute of Technology/Engineering, Wright-Patterson Air Force Base, OH 45433-6583.

U.S. Government work not protected by U.S. copyright.

---

0018-9251/95/\$4.00

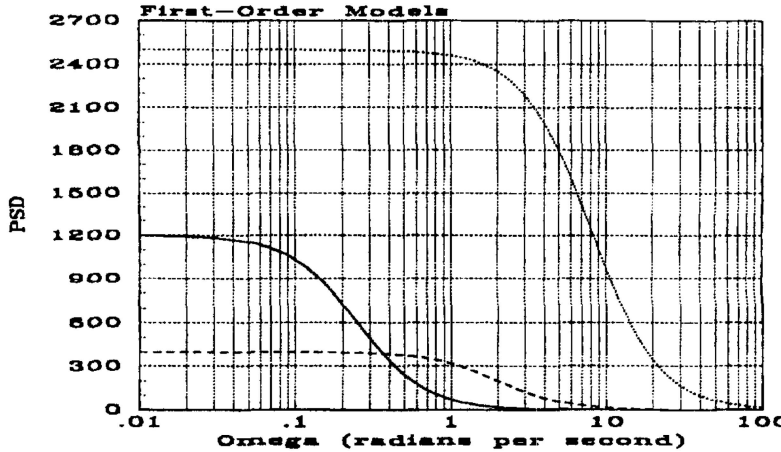


Fig. 1. Target acceleration PSD plots assumed by 3 possible elemental filter models.

could be used to process the raw FLIR data without a correlator preprocessor [15, 4, 12].

An MMAE form is used when the target dynamics are expected to change. In previous investigations, the MMAE had little trouble moving from an elemental filter tuned for benign target trajectories to one tuned for harsher trajectories when the target initiates a jinking maneuver. The problem comes when the target *returns* to a more benign trajectory. The MMAE takes longer to return to the elemental filter tuned for the more benign trajectory. It has been conjectured that part of this problem is due to the fact that, if target models have acceleration power spectral densities (PSDs) that overlap in the low-frequency region, as in Fig. 1, all models are able to represent such behavior by the actual target. On the other hand, when the target vehicle truly exhibits harsh maneuvering, only those models with non-zero acceleration PSD values over the higher frequencies can be deemed adequate [10]. In this investigation, the filter dynamics models are selected to produce elemental filters with nonoverlapping PSDs. First-order Gauss-Markov models, as produced by low-pass filters driven by white Gaussian noise, yield overlapping acceleration PSDs as in Fig. 1, despite the fact that higher break frequencies are meant to be indicative of more maneuverable characteristics. In contrast, the model parameters of second-order Gauss-Markov models using bandpass filters can be selected so that the PSDs have minimal overlap as in Fig. 4 (Section VI). The break frequency of the PSD is driven by how fast the target can change its velocity vector. The height of the PSD plot represents the mean square acceleration magnitude per unit frequency that the target is exhibiting and the overall height is determined by the dynamics driving noise of the filter model. The location and number of cutoff frequencies of the PSDs for the elemental shaping filters are additional design parameters to be varied for tuning to a given application.

## II. MMAE ALGORITHM

This section reviews the basic structure of the MMAE, highlighting features pertinent to this investigation. Full mathematical development of these concepts is found in Maybeck [8, p. 130]. The KF is a predictor/corrector algorithm. In the predictor function a model that describes the true system dynamics is propagated through one time increment, producing an estimate of states of interest of the true system. In this effort the true system dynamics are those displayed by the airborne target being tracked. The states of interest are the position, velocity, and acceleration of the target, and the apparent motion of the target due to atmospheric jitter. Certainly in this application many parameters describing the dynamics of motion of the target are unknown or can change over time. The target or its potential dynamics will not be known exactly *a priori*. However, there is a physical limit on the range of the dynamics a tracker can be expected to see. This range of possible dynamics is described by a parameter vector  $\mathbf{a}$ . This vector is discretized over its continuous space into  $j$  distinct points, each forming the basis of the predictor portion of an individual KF called an elemental filter.

The elemental filters are tied together in an MMAE as in Fig. 2. In this configuration, each of the  $j$  elemental filters propagates one time increment, producing an estimate of the states,  $\hat{\mathbf{x}}_k(t_i^-)$  for each  $k = 1, 2, \dots, j$ . Then the single measurement,  $\mathbf{z}(t_i)$ , is brought in and a residual,  $\mathbf{r}_k(t_i)$ , is calculated for each:

$$\mathbf{r}_k(t_i) \stackrel{\Delta}{=} \mathbf{z}(t_i) - \mathbf{H}_k(t_i) \hat{\mathbf{x}}_k(t_i^-) \quad (1)$$

where  $\mathbf{H}_k(t_i)$  is the measurement output matrix, and the minus sign in the superscript means before the measurement update. Now the MMAE can make an adaptive estimate of the state based on the characteristics of these residuals. A hypothesis conditional probability is calculated for each elemental filter being based on the most correct parameter value,

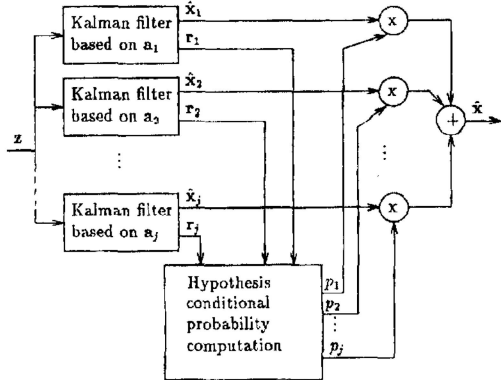


Fig. 2. MMAE structure [6, p. 132].

producing  $p_k(t_i)$ :

$$p_k(t_i) = \frac{1}{(2\pi)^{m/2}|\mathbf{A}_k(t_i)|^{1/2}} \exp\left\{-\frac{1}{2}\mathbf{r}_k^T(t_i)\mathbf{A}_k^{-1}(t_i)\mathbf{r}_k(t_i)\right\} p_k(t_{i-1}) \quad (2)$$

$$\sum_{g=1}^j \left[ \frac{1}{(2\pi)^{m/2}|\mathbf{A}_g(t_i)|^{1/2}} \exp\left\{-\frac{1}{2}\mathbf{r}_g^T(t_i)\mathbf{A}_g^{-1}(t_i)\mathbf{r}_g(t_i)\right\} p_g(t_{i-1}) \right]$$

where  $\mathbf{A}_k(t_i)$  is the computed residual covariance of the  $k$ th filter:

$$\mathbf{A}_k(t_i) = \mathbf{H}_k(t_i)\mathbf{P}_k(t_i^-)\mathbf{H}_k^T(t_i) + \mathbf{R}_k(t_i) \quad (3)$$

$\mathbf{P}_k(t_i^-)$  is the state estimate error covariance,  $\mathbf{R}_k(t_i)$  is the covariance of the measurement noise, and  $m$  is the number of measurements. There are two “measurements”,  $x$  and  $y$  position offsets in the FLIR image plane computed by the enhanced correlator. The sum of the probabilities is 1,  $\sum_{g=1}^j p_g = 1$ , because of the divisor in (2). The probability calculation is recursive. Since the current probability calculation includes the previous value, if the probability for any filter  $p_k$  goes to zero at one sample time, that probability will remain zero for all subsequent time increments. Tactics to prevent this lockout of a filter are varied [8, p. 130; 13, p. 18]. The one used here is the lower bound (a value of 0.001 is used). Each  $p_k$  is set to the lower bound if its calculated value is below that bound. Then the denominator in (2) is recalculated so the sum of probabilities will still be one.

The state estimate for the MMAE before measurement update is then:

$$\hat{\mathbf{x}}(t_i^-) = \sum_{k=1}^j p_k(t_i^-) \hat{\mathbf{x}}_k(t_i^-) \quad (4)$$

and similarly for the estimate after the measurement update at  $t_i^+$ . This is called a Bayesian MMAE estimate. A variation on this is the maximum a posteriori (MAP) estimate. In this case, the probabilities are calculated as in (2) and the MMAE estimate is set equal to the  $\hat{\mathbf{x}}_k(t_i)$  corresponding to the largest computed probability,  $p_k(t_i)$ .

The MMAE makes the adaptive estimate of the state based on the characteristics of the residuals. It is important that there be significant differences between residuals from the elemental filter designed for a specific trajectory and the other elemental filters so the correct elemental filter can be selected, that is, have the largest  $p_k(t_i)$ . Two things contribute to distinctive residuals among the elemental filters. First, the model upon which the filter is based must be specific for an expected trajectory. Hence the use of second-order Gauss-Markov models for acceleration. Each elemental filter is designed for a trajectory displaying a specific range of acceleration frequency

content. For example, how fast the plane responds to stick input will contribute to the frequency content of the resulting trajectory, as in the trajectory of an air superiority aircraft versus that of a cargo plane. Second, the filter must be tuned specifically for the expected trajectory. If pseudonoise is added, as in conservative tuning practices with nonadaptive filters [7, p. 339], it can blur the distinction between residuals of competing filters in the MMAE structure, and thereby incapacitate the adaptive mechanism of the MMAE algorithm [8, p. 133].

In addition to these two considerations, the MMAE algorithm itself will be altered in an attempt to affect elemental filter selection. The magnitude of the residuals squared comes into the  $p_k$  calculation in the exponential term as seen in (2). However, the residual covariance,  $\mathbf{A}_k(t_i)$ , enters into the exponential and the leading coefficient, potentially resulting in a larger  $p_k$  for the elemental filter that does not have the smallest magnitude residuals. For example, a filter tuned to expect harsh trajectories normally has larger dynamics noise strength. This makes the corresponding denominator  $|\mathbf{A}_k|$  tend to be of larger magnitude, while also making the term within the exponential a smaller magnitude negative number. The exponential terms thus make the probability calculation tend to favor the filter tuned for harsher trajectories when the residuals from several filters are of similar magnitude. However, the leading coefficient will be smaller for the larger  $|\mathbf{A}_k|$  and should counter the exponential. This particular trait of the probability calculation is suspect when the “wrong” elemental filter is selected in a particular application [8, 9, 17] and various “fixes” can be used. For example, Stevens [9, 17] suggested

removing the leading coefficient on the calculation of the conditional probability density that goes into the computation of the hypothesis conditional probability  $p_k$ , via (2) i.e., removing the terms preceding the exponentials in both numerator and denominator of (2), for a problem that caused the MMAE to show an artificial bias towards elemental filters with small  $|\mathbf{A}_k|$ . This suggestion may not be useful since, in the class of problems of interest in this research, one would like to enhance a bias toward elemental filters with small  $|\mathbf{A}_k|$ . The presence of the determinant in the leading coefficient would tend to counter the empirically observed sluggishness of the MMAE in returning to a benign-model elemental filter when a target vehicle stops maneuvering. However, an associated concept, called “maximum entropy” design [16], alters both the leading term and the exponential term by setting  $\mathbf{A}_k$  to  $\mathbf{I}$  in all filters (due to lack of confidence in the filter-computed  $\mathbf{A}_k$  values; the impact of  $\mathbf{A}_k$  is thereby removed) [10]. This may, in fact, prove useful in reducing the sluggishness of returning high probability to a benign-model elemental filter when a target stops maneuvering. Removal or nonremoval of the coefficient, and maximum entropy design, combined with use of elemental filters with nonoverlapping acceleration PSDs, should provide sufficient design freedom to improve tracking.

### III. TRUTH MODEL

The truth model is the model of the real world that creates the inputs for the MMAE. In this research the truth model must do the following two things:

- 1) The true position of the target image in the FLIR detector is simulated. The true position is used to determine how well the tracking algorithm works.
- 2) The truth model provides the measurements for the tracking algorithm to use as input. The measurements are the average intensity of IR radiation seen by each of the 64 pixels in the 8-by-8 “tracking window.” To generate this, the apparent location of the target is found. The apparent location is the sum of the true target position and the apparent position jitter due to atmospheric distortion of the IR wavefront. This measurement array is presented to the enhanced correlator. It generates a template from the 10 previous measurement frames and determines how much the center of intensity of the current measurement frame has moved from the center of intensity of the template. It is these offsets in the  $x$  (azimuth) and  $y$  (elevation) directions in the FLIR detector plane that are the measurements input to the MMAE algorithm.

A complete description of these is presented in [14]. Only pertinent aspects are presented here.

The target is maneuvering in an Earth-centered/Earth-fixed ( $\mathcal{I}$  or “inertial”) frame whose origin is

defined at the FLIR detector. The trajectories used in the investigation are *created* as a position vector in this inertial frame. Several trajectories are used. The airborne target stays at a constant altitude ( $z_{\mathcal{T}}$  direction) with constant velocity in the negative  $x_{\mathcal{T}}$  direction throughout the 6 s simulation. The motion dynamics are introduced in the  $y_{\mathcal{T}}$  direction via:

$$v_{\mathcal{T}y}(t) = A\omega \cos(\omega t + \phi) + B \text{ m/s.} \quad (5)$$

The amplitude  $A$  of the cosine wave would vary, limited by the maximum acceleration the manned target would pull. This acceleration due to the sinusoidal velocity can also be written

$$a_{\mathcal{T}y}(t) = A\omega^2 \sin(\omega t + \phi) \text{ m/s}^2. \quad (6)$$

The bias  $B$  and phase  $\phi$  variables are used in more elaborate trajectory construction; for example, creating a target pulling a jinking maneuver in the velocity domain so that it will not have discontinuities in acceleration [14]. This velocity vector is projected onto a two-dimensional position vector in the detector plane, ( $x_D$  and  $y_D$ ).

The image of the target in the detector frame will undergo apparent motion due to the IR wavefront propagating through the atmosphere. The model used for this was developed by The Analytical Sciences Corporation [19] and is discussed in [11, p. 10]. The mathematical model for atmospheric jitter is a three-state linear shaping filter driven by unit-strength zero-mean white Gaussian noise. The transfer function is

$$\frac{y_{ta}}{w_{ta}} = \frac{Kab^2}{(s+a)(s+b)^2}. \quad (7)$$

The poles and other important parameters are

$$a = 14.14 \text{ rad/s}$$

$$b = 659.5 \text{ rad/s}$$

$$K = 0.382109544\sigma_{ta}$$

$$\sigma_{ta} = 0.447.$$

The variable,  $\sigma_{ta}$ , is the standard deviation of the output  $y_{ta}$ . The subscript  $ta$  refers to the true atmospheric model. Mercier calculated the gain  $K$  [11, p. 76]. The jitter effect is assumed independent of the direction of interest in the detector plane, so the state-space model is developed independently in each  $x_D$  and  $y_D$  direction.

### IV. ELEMENTAL FILTER DESIGN

Models are developed to describe the atmospheric jitter and the target acceleration process. From these models, the appropriate matrices for the KF equations are generated. The models are developed in the continuous-time domain, then the equivalent discrete-time version is found [14].

The atmospheric jitter for the filter equations is modeled as a stationary first-order Gauss-Markov process. This is the output of a first-order lag driven by white Gaussian noise of strength  $q$  [7, p. 184]. The differential equation for the first-order lag model is  $\dot{x}(t) = (-1/T)x(t) + w(t)$  with noise described with  $E\{w(t)\} = 0$  and  $E\{w(t)w(t + \tau)\} = q\delta(\tau)$  where  $q = 2\sigma^2/T$ . The correlation time is  $T$  and the mean squared value of the output is  $\sigma^2$ . The appropriate values are  $T_{fa} = 0.0707$  s and  $\sigma_{fa}^2 = 0.2$  pixels<sup>2</sup> in each direction. The subscript  $fa$  denotes the filter atmospheric model. The jitter is created in the truth model with three states. In the interest of keeping the number of states down, the filter tracks only the dominant single pole at  $1/T_{fa}$  or 14.14 rad/s.

Two kinds of acceleration models are developed. The acceleration can be modeled as a first-order Gauss-Markov process, leading to three filter states for each axis in the detector plane:

$$\begin{aligned}\dot{p}(t) &= v(t) \\ \dot{v}(t) &= a(t) \\ \ddot{a}(t) &= (-1/T)a(t) + w(t)\end{aligned}\quad (8)$$

where the noise is zero-mean with strength of  $q = 2\sigma^2/T$ . The variables,  $p$ ,  $v$ , and  $a$  are position, velocity, and acceleration, respectively. The values for  $T_{fm}$  and  $\sigma_{fm}^2$  are selected for each elemental filter. The subscript  $fm$  denotes the filter model of actual target motion (versus apparent motion due to atmospheric jitter, with subscript  $a$ ). This acceleration model has been implemented in this particular tracker many times before [5, 6, 18, 20].

The target acceleration process can alternately be modeled as a second-order Gauss-Markov process by driving a second order linear system with unit-strength zero-mean white noise [7, p. 185]. Four states for each direction are required to model the motion rather than the three of the previous model. A two-pole transfer function is selected that will model an acceleration process with an appropriate PSD selected by the researcher. This transfer function can have two real poles or a complex pair. Matrix-X [2] is used to find a corresponding state space form, and desired steady state conditions are established. The two-state acceleration model is augmented with the position and velocity model and the model is applied to both axes yielding the eight-state state vector:

$$\mathbf{x}_{fm} = \begin{bmatrix} p_{fmx} \\ p_{fmy} \\ v_{fmx} \\ v_{fmy} \\ b_{fmx} \\ b_{fmy} \\ c_{fmx} \\ c_{fmy} \end{bmatrix} \quad (9)$$

where the variables  $b$  and  $c$  are the two states that together generate a scalar acceleration output. Augmentation with the two atmospheric states is then accomplished so that the proper  $\mathbf{H}_f$  matrix is  $[\mathbf{I}_{2 \times 2} \ \mathbf{0}_{2 \times 6} \ \mathbf{I}_{2 \times 2}]$ .

## V. SIMULATION PRODUCTS

Two kinds of MMAEs are of interest here. One has elemental KFs based on first-order Gauss-Markov models for acceleration. The second MMAE has a mix of elemental filters, some based on first-order Gauss-Markov acceleration models, and some based on second-order Gauss-Markov acceleration models.

The performance of the MMAEs is evaluated by calculating the statistics of the errors committed by the filter in estimating the states. The error is the estimate from the MMAE minus the state from the truth model. For this investigation, a Monte Carlo study is accomplished to get these values. In a Monte Carlo study, many samples of the error are simulated and the sample statistics are computed [7, p. 329]. An infinite number of samples are required to get the true statistics of the stochastic process model. However, usually a smaller number of samples will converge to a value that is close to the true value. Previous investigations [11, p. 43; 3, p. 28; 1, pp. 26, 33] have shown acceptable convergence in 10 runs.

The mean error is calculated as [17, p. V-3]:

$$\bar{E}(t_i) = 1/N \sum_{n=1}^N [x_t(t_i) - \hat{x}_f(t_i)] = 1/N \sum_{n=1}^N e(t_i) \quad (10)$$

with the variance given by

$$\sigma^2(t_i) = \frac{1}{N-1} \sum_{n=1}^N e^2(t_i) - \frac{N}{N-1} \bar{E}^2(t_i) \quad (11)$$

where  $N$  is 10. The mean error is  $\bar{E}(t_i)$  while the error for one run of the Monte Carlo study at one time  $t_i$ , is  $e(t_i)$ . Possible values of the generic true and filter-computed variables  $x_t$  and  $x_f$  are the position of the target (denoted  $p_x$  and  $p_y$ ) and apparent position of the centroid (denoted  $y_x$  and  $y_y$ ) in the detector plane, i.e., the sum of target position states and jitter position states. Error statistics are kept at each  $t_i^-$  and  $t_i^+$  and for each of the  $x$  and  $y$  directions in the detector plane. The statistics are evaluated in two forms, a plot of the data versus  $t_i$  or a temporal average from 0.5 s to the end of the run. The average is started at a half second so the initial transients do not affect the averages.

Also available from each Monte Carlo study is information on the magnitude of  $\mathbf{r}_k^T(t_i)\mathbf{r}_k(t_i)$ ,  $\mathbf{r}_k^T(t_i)\mathbf{A}_k^{-1}(t_i)\mathbf{r}_k(t_i)$ , the leading coefficient of the  $p_k$

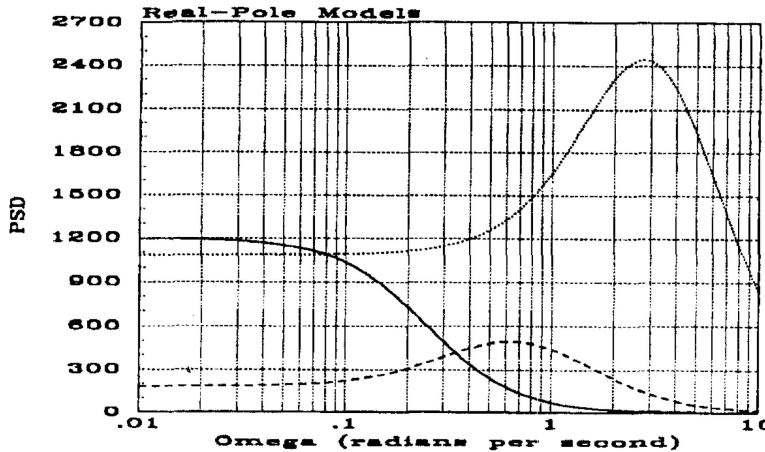


Fig. 3. PSD plot of real-pole MMAE.

calculation, and the time history of the  $p_k$  calculation. Recall that the relative magnitudes of first three terms determine which elemental filter will have the largest  $p_k$  assigned. This probability calculation is one of several characteristics of the MMAE algorithm being investigated to determine how best to help the MMAE select the correct elemental filter for tracking a particular target. To aid this investigation, these terms are evaluated separately.

## VI. PERFORMANCE EVALUATION

Manned aircraft will show a range of frequency content for acceleration. A cargo plane traveling straight and level will have an acceleration that shows power in a PSD below a cutoff of 0.25 rad/s ( $T_{fm} = 4$  s). An air superiority craft pulling evasive maneuvers can show power at frequencies greater than a cutoff of 1.3 to 1.7 radians per second. Manned craft should show no power content above a frequency cutoff of about 2.5 rad/s [10]. This readily translates to three elemental filters. One is based on an acceleration model that is a low-pass filter with cutoff at 0.25 rad/s. It is referred to as the “benign” filter. This is the same benign filter used by previous investigations [18, p. 69; 5, p. 67]. The second, called the “intermediate” filter, is centered between 0.25 and 0.8 rad/s. The last, the “harsh” filter, is centered between about 0.6 and 2.5 rad/s. The second-order filters are designed within these rough limits.

In order to tune each of these three filters created with an acceleration model having a particular frequency range in mind, a trajectory showing an acceleration with that frequency, as described in (5), is used. These three trajectories are called “basic” to the particular MMAE because they are the frequencies about which the PSDs of the elemental filter models are centered. A tuned value of  $q$  is selected for each elemental filter by tracking each trajectory with the appropriate elemental filter only (not the MMAE).

The initial second-order filter investigated was the filter based on an acceleration model with two real poles. The transfer function  $G(s)$  describing the acceleration model that is the basis for the intermediate filter is

$$G(s) = \frac{1.715(s + 0.1768)}{(s + 1.4305)(s + 0.3531)} \quad (12)$$

The transfer function describing the acceleration model that was the basis for the harsh filter is

$$G(s) = \frac{5.2(s + 1.0111)}{(s + 2.0222)(s + 5)}. \quad (13)$$

The result of this investigation was similar to using three first-order elemental filters in the MMAE. This was attributed to the similarities in the PSD plots at the low frequency end. That is, the PSD of the model for the harsh filter encompasses the benign and intermediate model PSDs, as shown in Fig. 3.

The potential for overlap is inherent in a real-pole model when the dynamics driving noise strength is as high as was deemed necessary for tuning of each elemental filter. Therefore, a notch filter was designed. The notch filter is based on an acceleration represented as the output of a white-noise-driven linear model with the transfer function:

$$G(s) = \frac{ks}{s^2 + 2\zeta\omega_t s + \omega_t^2} \quad (14)$$

where  $\zeta$  was 0.2 and  $\omega$  for the intermediate and harsh filters were 0.62 and 2.8 rad/s, respectively. The small  $\zeta$  gave minimal overlap of the PSD plots for the benign and intermediate filters. The  $\omega$ s selected centered the notch filters at the same frequencies as the real pole filters were centered. These were tuned in the manner described above.

The MMAE thus designed was allowed to track each basic trajectory. However, the probability plots showed almost identical traces for the benign and intermediate trajectories. The benign and intermediate filter models were not different enough from each

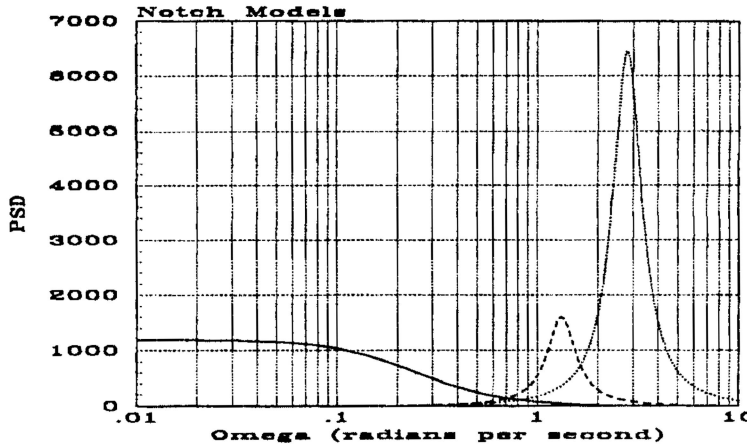


Fig. 4. PSD plot of MMAE with notch elemental filter models.

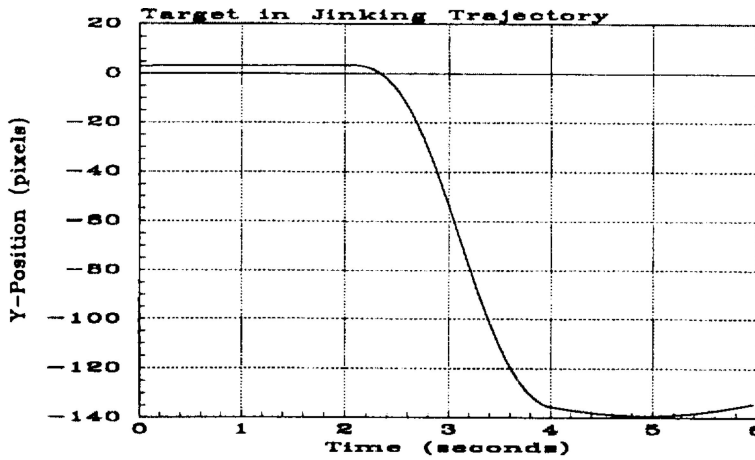


Fig. 5. Target position; detector plane; jinking trajectory.

other to track their basic trajectories. Therefore, a new intermediate filter was chosen based on an acceleration model that shows a peak at  $\omega = 1.32$  rad/s in a PSD plot. The MMAE with this new elemental filter was designated “–2.” The peak fell between the peaks for the models at 0.62 and 2.8 rad/s. The filter was tuned for a trajectory with  $\omega = 1.32$  rad/s and an amplitude of 9 m. A plot of the tuned MMAE-2 is shown in Fig. 4.

This “notch MMAE-2” was allowed to track targets undergoing accelerations with frequencies of 0.01, 1.32, and 2.8 rad/s. The probability plots are in Fig. 7; to be discussed more fully later. This notch filter is used for the probability calculation analysis.

As a result of these efforts, we finally see a proper difference in elemental filter selection when the MMAE is tracking the benign and the intermediate trajectories. The harsh filter remains uncontested in tracking the harsh trajectory. The benign filter attains the highest probability on the benign trajectory after about 0.6 s. There is a lot of switching between the benign and intermediate filters for the intermediate trajectory. The times of switching, 0.6, 1.1, 1.7, and 2.5 s are not related to anything obvious in the

trajectory acceleration. The average  $\mathbf{r}_k^T(t_i)\mathbf{r}_k(t_i)$  is smaller for the intermediate filter but the leading coefficient in the probability calculation gives the benign filter an advantage due to its smaller magnitude dynamics driving noise strength. The y position rms error plot showed ripples due to filter switching. There are trajectory trends remaining in the y position error plots for both the intermediate and harsh trajectories, still of a small magnitude, less than half a pixel for the  $t_i^+$  plots. This is due to less-than-optimal state estimation by the filter.

The trajectories considered thus far were tied to the elemental filters in the MMAE as we investigate filter selection. In other words, the simulated “real world” was one of the three nominal trajectories for all 6 s of the simulation. A trajectory was created to simulate a target in an evasive maneuver by concatenating 2 s of each nominal trajectory type together. As with the basic trajectories used above, the motion dynamics were added only to the y direction. The y position in the detector plane for this jinking motion is shown in the plot in Fig. 5. In the inertial frame the target experiences about 7.3 gs acceleration in the dive.

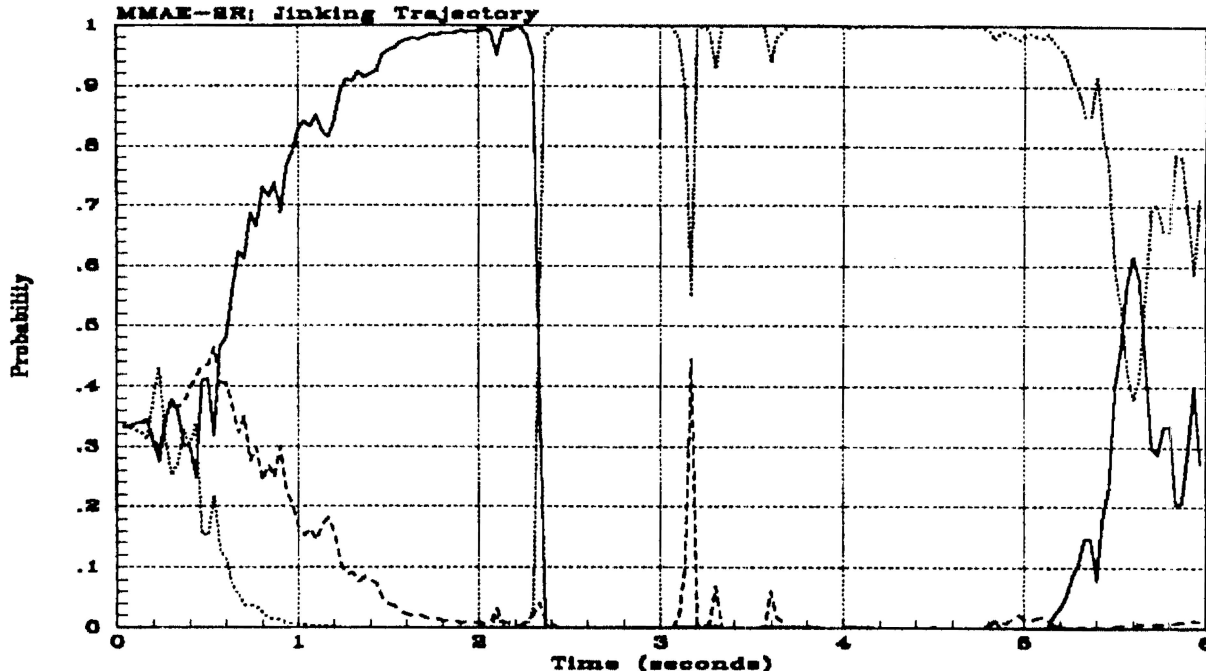


Fig. 6. Probability plots; notch MMAE-2; jinking trajectory. Benign filter, solid line; intermediate filter, dashed line; harsh filter, dotted line.

The “notch MMAE-2” was allowed to track this trajectory, giving the probability plot of Fig. 6. The first part of the trajectory was benign. Thus the probability plots match pretty well the corresponding probability plots for the benign trajectory in Fig. 7. The diving part of the trajectory was a piece of the harsh trajectory so it is expected that the harsh filter would be selected for that part. As seen in Fig. 5, the harsh trajectory was inserted at 2 s but care was taken by using the phase and bias variables in the velocity equation of (6) to ensure no discontinuities in the acceleration or jerk domains. Therefore, the target slowly fell into the dive and filter selection was delayed for about 0.3 s, as seen in Fig. 6. At 4 s, the trajectory with  $\omega = 0.62 \text{ rad/s}$  was inserted. This is evident in the trajectory plot in Fig. 5, but filter selection did not begin to change until past 5 s. The benign filter was being selected when the simulation ended.

#### A. Examining the Hypothesis Probability Calculation

As discussed in Section II, there are alternatives in the way the hypothesis probability is calculated. The probability calculation is given in (2). It is proposed to set  $\mathbf{A}_k(t_i)$  equal to  $\mathbf{I}_{2 \times 2}$  in the exponential, in the leading coefficient, or in both. This leads to four cases.

1) Use the traditional calculation as in (2) and (3) as has been done thus far. At issue here is that, when the residuals of each of the elemental filters are such that the exponentials in (2) are of the same magnitude, the leading coefficient causes the MMAE to select the “more benign” filter because it tends to have the

smaller dynamics driving noise and thus the smaller  $|\mathbf{A}_k(t_i)|$ . However, the  $\mathbf{A}_k^{-1}(t_i)$  in the exponential causes the calculation to favor the “harsher” elemental filter because it has the greater dynamics driving noise. This investigation will help in deciding if removing one or both of the  $\mathbf{A}_k(t_i)$ s will aid in tracking.

2) Leave the leading coefficient as it is in (2), but set  $\mathbf{A}_k(t_i)$  equal to  $\mathbf{I}_{2 \times 2}$  in the exponential. This should enhance the ability to return high probability to the benign elemental filter when a target stops maneuvering and returns to a benign flight trajectory.

3) Remove the leading coefficient. Setting  $\mathbf{A}_k(t_i)$  to  $\mathbf{I}_{2 \times 2}$  in the leading coefficient would leave a constant multiplier that is the same for all elemental filters. The multiplier is set to one which will allow the *exponential* term to select the “correct” elemental filter when the residuals from each are about the same magnitude. The MMAE should favor the “harsh” filter.

4) Remove the leading coefficient and set  $\mathbf{A}_k(t_i)$  equal to  $\mathbf{I}_{2 \times 2}$  in the exponential. This is the maximum entropy application discussed in Section II. Only residual magnitudes (absolute magnitudes, not scaled relative to anticipated rms residual size) will determine filter selection.

Each of these probability calculations is referenced in the sequel by case number, as given above.

The notch MMAE-2 is allowed to track its basic trajectories with each of the four hypothesis probability calculations, resulting in the probability plots of Figs. 7–10. The probability plot for Case 2 in Fig. 8 shows the benign filter selected more for the benign

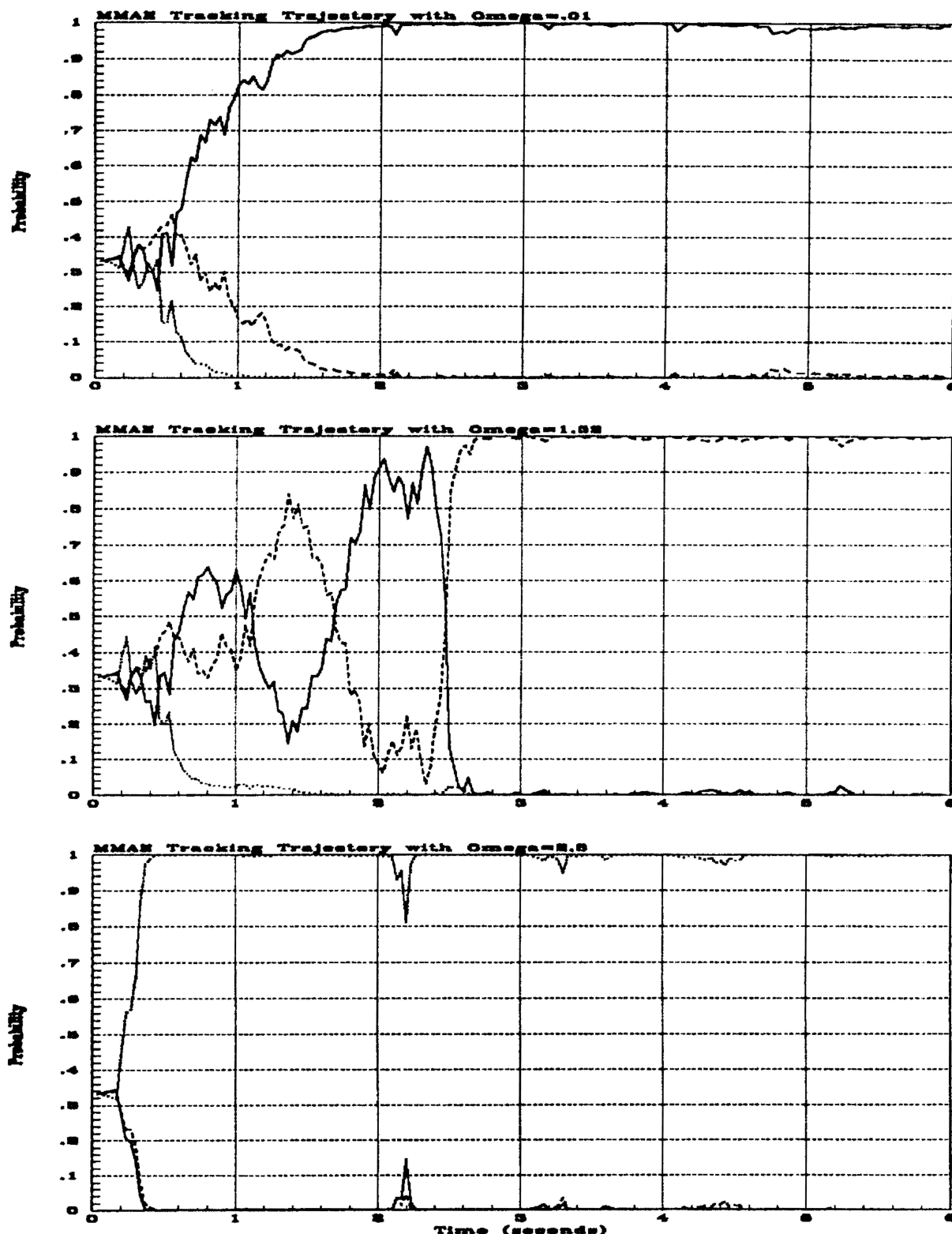


Fig. 7. Probability plots; notch MMAE-2; basic trajectories. Benign filter, solid line; intermediate filter, dashed line; harsh filter, dotted line.

and intermediate trajectories. This is expected because the magnitude of the residuals,  $\mathbf{r}_k^T(t_i)\mathbf{r}_k(t_i)$ , in the exponential is about the same whether tracked by the benign or intermediate filters. The determining factor will then be the leading coefficient. The leading

coefficient is greater for the filter with the weakest dynamics driving noise. The harsh trajectory is tracked by the harsh filter because, by far, it gives the smallest magnitude of residuals. The error plot shows an increased magnitude for the first 0.5 s because of the

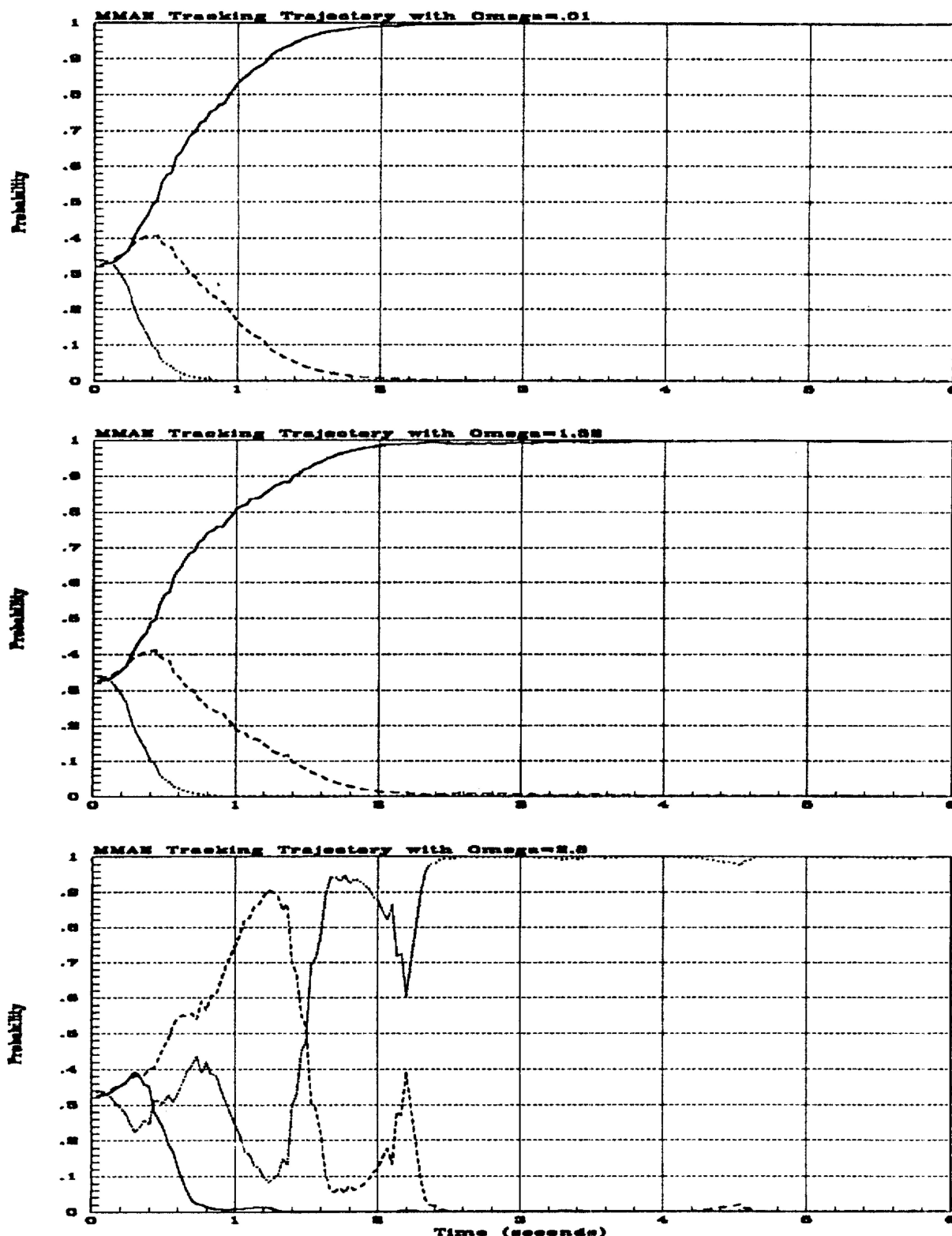


Fig. 8. Probability plots; notch MMAE-2, Case 2; basic trajectories. Benign filter, solid line; intermediate filter, dashed line; harsh filter, dotted line.

nontrivial (and inappropriate) contribution of the benign filter.

The probability plots of the study of Case 3 in Fig. 9 shows the harsh filter tracking all the trajectories. This is expected since the leading

coefficient is removed. The leading coefficient tends to be smallest for the harshest filter while the magnitude of the  $\mathbf{r}_k^T(t_i)\mathbf{A}_k^{-1}(t_i)\mathbf{r}_k(t_i)$  that remains in the exponential is smallest for the harsh filter. This makes the probability the largest for the filter with

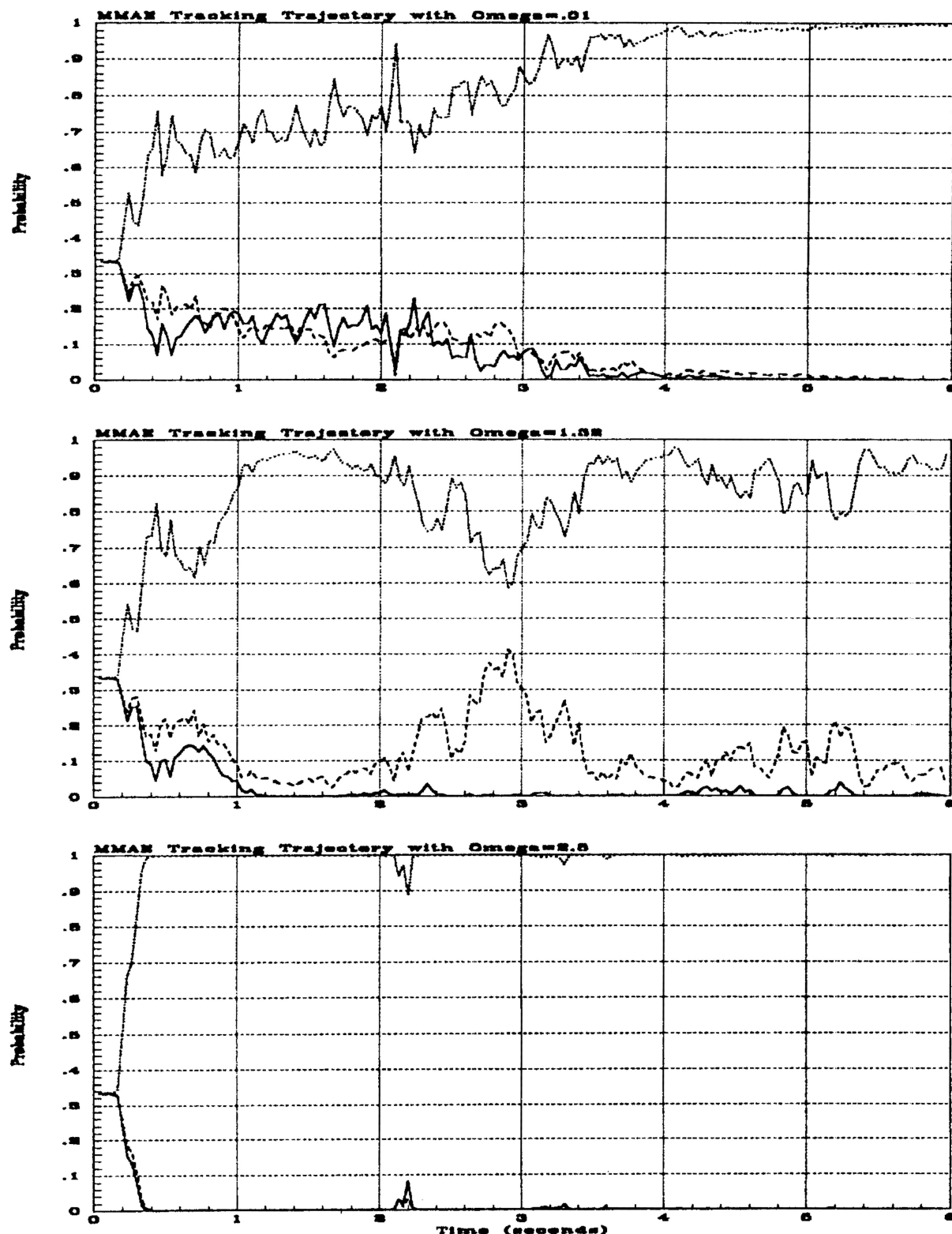


Fig. 9. Probability plots; notch MMAE-2; Case 3; basic trajectories. Benign filter, solid line; intermediate filter, dashed line; harsh filter, dotted line.

the greater dynamics driving noise strength when the residuals are not very different between elemental filters. Because the harsh filter does all the tracking, the standard deviations of the errors are greater than for the MMAE for Case 1.

The probability plots for Case 4 in Fig. 10 look much like the plots for Case 1 except with a much slower response. The benign and intermediate filters fight for both the benign and intermediate trajectories.

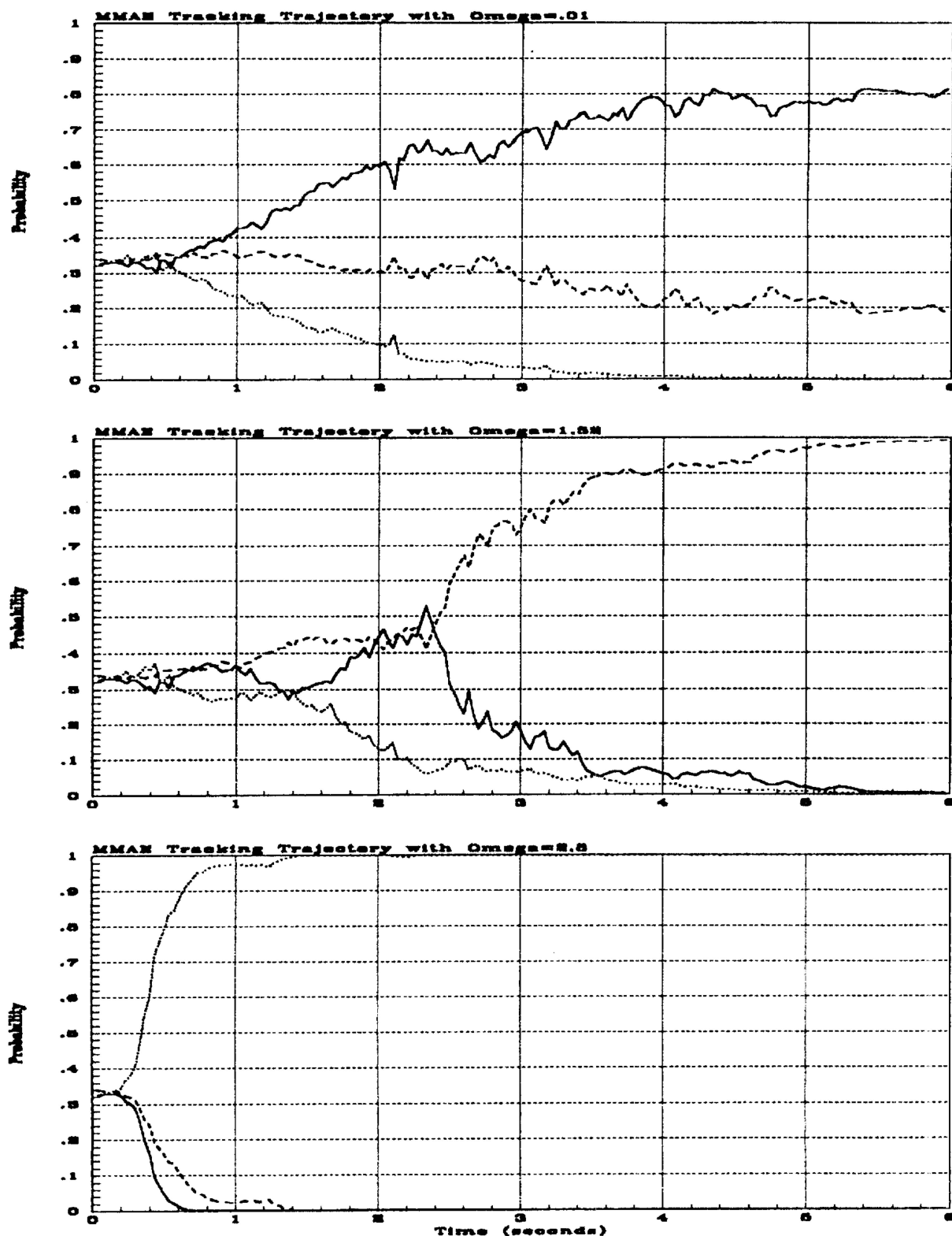


Fig. 10. Probability plots; notch MMAE-2; Case 4; basic trajectories. Benign filter, solid line; intermediate filter, dashed line; harsh filter, dotted line.

Given these probability plots and these *nonvarying* trajectories, Case 2 or 4 would be acceptable. There is less switching, the harsh filter does track the harsh trajectory (the hardest job), and either the benign or intermediate filters (or both) show adequate

performance tracking either the benign or intermediate trajectories. The slow response time that makes these plots look so smooth would make these probability computation options unacceptable in tracking an evading target that exhibits a range of trajectory

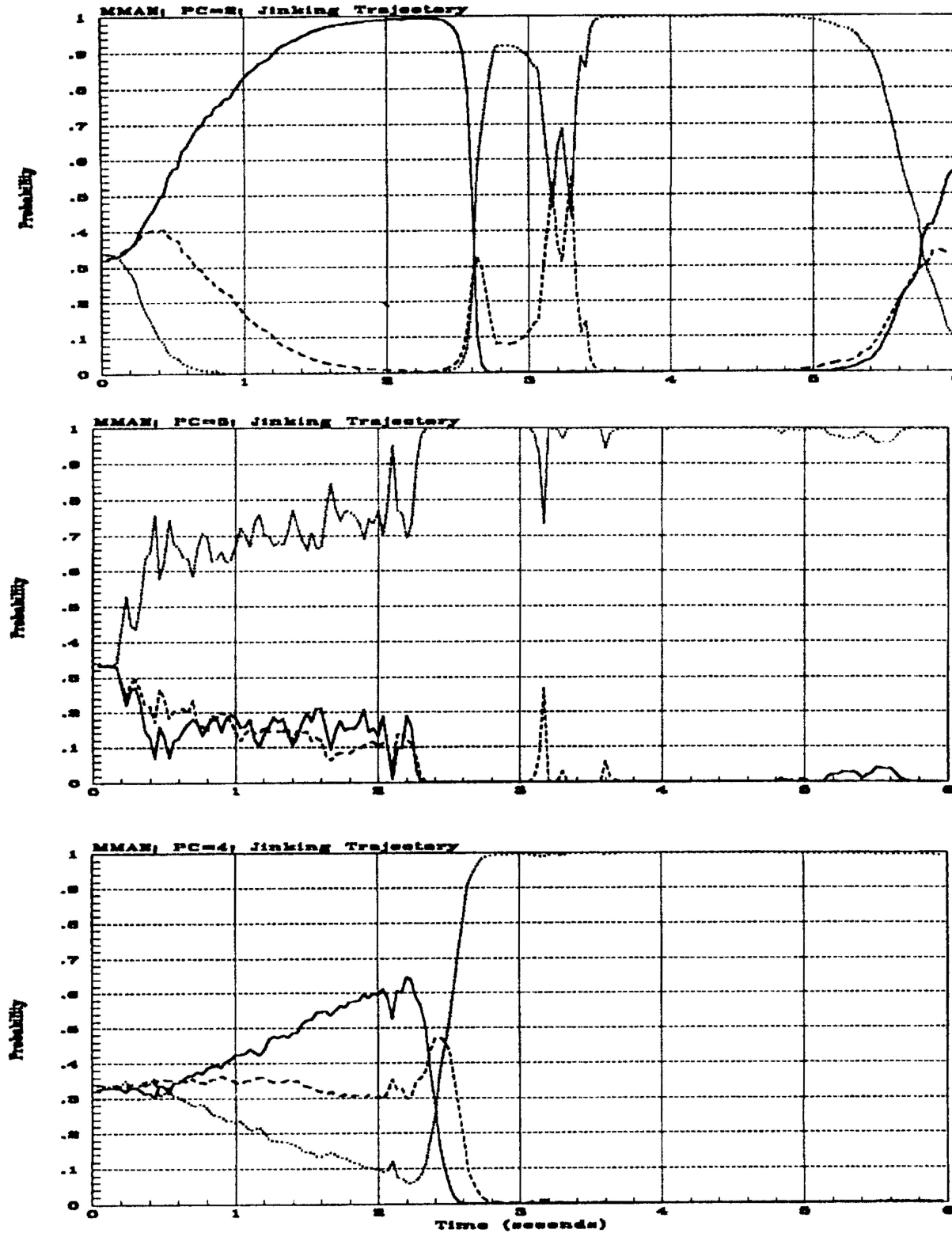


Fig. 11. Probability plots; notch MMAE-2; Case varied; jinking trajectories. Benign filter, solid line; intermediate filter, dashed line; harsh filter, dotted line.

characteristics in a short time period. Thus, Case 1 would be preferred.

The notch MMAE-2 is allowed to track the jinking trajectory using Cases 2, 3, and 4. The probability plots are in Fig. 11. Recall, the probability plot for the notch

MMAE-2 for Case 1 tracking the jinking trajectory is in Fig. 6.

For Case 2, the probability plot looks very similar to the probability plot for Case 1, except that the switch from the benign to harsh filter after 2 s is

TABLE I  
Average Position Errors for First-Order (FO) and Notch (N2) MMAEs. Cases 1 and 4

Traj $\omega$	Error in:						MMAE, Case
	$p_x(t_i^-)$	$p_x(t_i^+)$	$y_x(t_i^-)$	$p_y(t_i^-)$	$p_y(t_i^+)$	$y_y(t_i^-)$	
.01	.159±.408	.121±.371	.098±.381	.005±.347	.006±.315	.011±.366	FO,1
.01	.114±.422	.086±.381	.071±.385	.003±.361	.003±.325	.008±.370	FO,4
.01	.164±.411	.126±.373	.103±.381	-.004±.347	-.003±.314	.002±.366	N2,1
.01	.098±.427	.081±.387	.065±.388	.004±.362	.004±.326	.008±.372	N2,4
1.32	.058±.447	.034±.398	.043±.395	-.002±.408	-.007±.361	-.008±.383	FO,1
1.32	.063±.443	.040±.394	.046±.392	-.026±.401	-.029±.355	-.021±.380	FO,4
1.32	-.033±.445	-.028±.396	-.016±.392	-.008±.391	-.014±.343	-.016±.374	N2,1
1.32	-.026±.444	-.017±.396	-.010±.391	-.014±.389	-.023±.343	-.014±.378	N2,4
2.8	-.023±.559	-.024±.446	-.010±.446	.013±.498	-.003±.386	.008±.429	FO,1
2.8	-.016±.560	-.018±.447	-.003±.446	.027±.501	.007±.389	.019±.429	FO,4
2.8	-.096±.512	-.060±.431	-.061±.420	.066±.450	.028±.371	.047±.403	N2,1
2.8	-.093±.509	-.058±.429	-.058±.420	.086±.453	.043±.373	.062±.402	N2,4
Jink	.035±.497	.018±.412	.031±.419	.025±.459	.017±.376	.021±.409	FO,1
Jink	.003±.509	-.007±.420	.012±.425	.063±.473	.012±.385	.041±.415	FO,4
Jink	-.009±.471	-.005±.408	.001±.406	.137±.425	.087±.361	.106±.393	N2,1
Jink	-.038±.482	-.025±.416	-.015±.411	.151±.435	.095±.370	.110±.396	N2,4

delayed by almost 0.3 s, as is the switch from harsh to benign after 5 s. The plot does show the desired improvement in removing high probability from the harsh elemental filter from  $t = 4.0$  s on, but at the expense of the intermediate one contributing to the MMAE estimate during  $t = 2.6$  to 3.6 s. The Case 3 option causes the MMAE to select only the harsh filter. For Case 4, the switch after 2 s is delayed and the one after 5 s did not even take place. Using this option appears to disable the MMAE and it cannot make a decision, even a wrong one, quickly. Given these responses, only the Case 1 option is acceptable.

### B. MMAE Based on First-Order Models

Since previous research has used first-order acceleration models, a comparison must be made to determine which MMAE tracks better, one with all elemental filters based on first-order acceleration models or the MMAEs with some of the elemental filters based on second-order models. One “first-order” MMAE is designed. The elemental filters have the correlation times of 4, 0.5, and 0.125 s for the benign, intermediate, and harsh filters, respectively. These values place the break frequency for the intermediate filter between the peaks for the intermediate and harsh notch models. The break frequency for the harsh filter is slightly above the peak of the harsh notch model. The lower bound for the probability calculation is held at 0.001. The MMAE is used to track the basic trajectories, those with  $\omega_s$  of 0.01, 1.32, and 2.8 rad/s, and the jinking trajectory. The PSD plot for these acceleration models is that presented in Fig. 1. Only the probability calculation options 1 and 4 are used (as described in Section VI-A) while tracking the basic trajectories and the jinking maneuver.

The probability plots for the first-order MMAE are almost identical to that of the notch MMAE-2 for either probability calculation option and any trajectory and so are not presented. There is no difference in

the mean position error magnitudes relative to the magnitude of the standard deviations over the 10 Monte Carlo runs between the two kinds of MMAE or the two probability calculation options. Table I shows a compilation of the average position errors for the four Monte Carlo studies. The key comparison is for probability calculation Case 1 since that option yields an MMAE that gives the best performance with regard to filter selection. For the intermediate trajectory, the notch MMAE-2 has smaller mean errors. For the harsh trajectory, the first-order MMAE has smaller mean errors but slightly larger standard deviations. Neither the first-order MMAE nor the notch MMAE-2 outperforms the other based on the criteria used for the evaluation.

### C. Proximity Check for Filters

There is some difficulty defining an intermediate filter that will allow the MMAE to select the “correct” elemental filter for a particular trajectory. The elemental filters were initially defined by what is known about how major classes of manned aircraft perform. This proved inappropriate despite the various modifications applied to the MMAE in this research. These difficulties motivate a proximity check to determine how practically the parameter space could be divided for a three-filter MMAE. The issue is, how much acceleration PSD overlap is permissible before elemental filter selection becomes inappropriate or ambiguous? In other words, how much separation between notched PSD regions should be maintained in order to generate unambiguous and correct filter selections?

The first difficulty encountered was the MMAE selecting the benign filter to track a simulated trajectory that should have yielded high probability weight for the intermediate notch filter. This benign filter is needed in the MMAE because any airborne target is capable of presenting a trajectory with

acceleration power in the low frequency range, as in a level flyby. Therefore, the benign filter will be held constant and the intermediate notch filter is moved to higher frequencies. Two more intermediate filters are defined, resulting in a MMAE-3 with  $\omega_{i3} = 1.92$  rad/s and a MMAE-4 has  $\omega_{i4} = 2.32$  rad/s. For a performance check, only the benign and intermediate filters are allowed to contribute to the MMAE while it tracks a target with the respective newly defined intermediate trajectory. For both the notch MMAE-3 and MMAE-4, the benign filter probability fell to 0.2 within the first half second and only the intermediate filter contributed to the estimate thereafter.

An obvious remaining point to investigate is, how “close” can the intermediate and harsh notch filter models get in their PSD representation and still track the intermediate and harsh trajectories? To this end, MMAEs 2, 3, and 4 are allowed to track their respective intermediate trajectory, the harsh trajectory, and a sinusoidal trajectory with an  $\omega$  between the PSD representation of the filter models, called the middle trajectory.

In both the notch MMAE-2 and the notch MMAE-3, the harsh filter is selected to track the harsh trajectory and not the intermediate trajectory. In the notch MMAE-2, the middle trajectory is tracked by both notch elemental filters; neither is more “correct”. In contrast, the notch MMAE-3 and the notch MMAE-4 each select the intermediate filter to track their respective middle trajectories and the latter MMAE selects the intermediate filter to track even the harsh trajectory. This latter MMAE has the intermediate and harsh elemental filter models designed too closely in the parameter space. Notch MMAE-3 gives better performance for filter selection.

## VII. CONCLUSIONS

The parameter space is suitably discretized with the notch MMAE-2 or the notch MMAE-3. These are three-elemental-filter MMAEs, each with a benign filter based on a first-order acceleration model ( $T = 4$  s) and a harsh filter based on a notch acceleration model ( $\omega = 2.8$  rad/s). The intermediate filter is based on a notch model with  $\omega = 1.32$  rad/s for notch MMAE-2 or  $\omega = 1.92$  rad/s for notch MMAE-3. In comparison, the first-order MMAE is designed with break frequencies ( $T$  is 4, 0.5, and 0.125 s for the three elemental filters) close to the roll-off frequencies of the notch MMAE-2 and the resulting models also represent a suitable discretization. The suitability of the discretization can be corrupted by improper tuning.

The probability calculation option that gives acceptable results with regard to both filter selection and error magnitudes is 1 (the “basic” hypothesis probability calculation). The maximum entropy option allows the MMAE to take too long to select an elemental filter clearly. The errors increase for

this option with the harsher trajectories because the more benign filters are allowed to affect the MMAE estimate too much.

The MMAE based on the first-order acceleration models performs basically the same as the MMAE based on the second-order models. The standard deviation of the position errors are somewhat smaller for the notch MMAE but the magnitudes of the mean errors are about the same for each MMAE over all the trajectories tested.

The greatest motivation for trying the second-order filter models (and looking at the acceleration models in the frequency domain of the PSD plot) was to get an MMAE that would assign greater probability to a filter based on a less harsh model more quickly after a target stops maneuvering. This happened with Case 1 in Fig. 6 and somewhat with Case 2 in Fig. 11. The first-order MMAE appears to do this as well as the second-order MMAE, while still having reasonable error magnitudes and an acceptable probability time history through the whole simulation. Since it entails lower computational loading, the first-order MMAE would be preferable.

## REFERENCES

- [1] Flynn, P. M. (1981) Alternative dynamics models and multiple model filtering for a short range tracker. MS thesis, AFIT/GE/ENG/81D, School of Engineering, Air Force Institute of Technology (AU), Wright-Patterson AFB, OH, Dec. 1981. Also DTIC Acc. No. ADA115503.
- [2] Integrated Systems Incorporated (1988) *Matrix-X*. Matrix Analysis Package Version 7.0, Santa Clara, CA 95054-1215, Oct. 1988.
- [3] Jensen, R. I., and Harnly, D. A. (1979) An adaptive distributed-measurement extended Kalman filter for a short range tracker. MS thesis, AFIT/GA/EE/79-1, School of Engineering, Air Force Institute of Technology (AU), Wright-Patterson AFB, OH, Dec. 1979. Also DTIC Acc. No. ADA080249. (See also Maybeck, P. S., Jensen, R. L., and Harnly, D. A. (1981) An adaptive extended Kalman filter for target image tracking. *IEEE Transactions on Aerospace and Electronic Systems*, AES-17, 2 (Mar. 1981), 172–180.)
- [4] Kozemchak, M. R. (1982) Enhanced image tracking: Analysis of two acceleration models in tracking multiple hot-spot images. MS thesis, AFIT/GE/ENG/82D, School of Engineering, Air Force Institute of Technology (AU), Wright-Patterson AFB, OH, Dec. 1982. Also DTIC Acc. No. ADA124781.
- [5] Leeney, T. A. (1987) A multiple model adaptive tracking algorithm against airborne targets. MS thesis, AFIT/GE/ENG/87D-37, School of Engineering, Air Force Institute of Technology (AU), Wright-Patterson AFB, OH, Dec. 1987. Also DTIC Acc. No. ADA190619.
- [6] Loving, P. A. (1985) Bayesian vs. MAP multiple model adaptive estimation for field of view expansion in tracking airborne targets. MS thesis, AFIT/GE/ENG/85M, School of Engineering, Air Force Institute of Technology (AU), Wright-Patterson AFB, OH, Mar. 1985. Also DTIC Acc. No. ADA155466.

- [7] Maybeck, P. S. (1979) *Stochastic Models, Estimation, and Control*, Vol. I. New York: Academic Press, 1979.
- [8] Maybeck, P. S. (1982) *Stochastic Models, Estimation, and Control*, Vol. II. New York: Academic Press, 1982.
- [9] Maybeck, P. S., and Stevens, R. D. (1990) Reconfigurable flight control via multiple model adaptive control methods. In *Proceedings of the IEEE Conference on Decision and Control*, Dec. 1990, p. 3551.
- [10] Maybeck, P. S. (1991) Personal interviews. AFIT, Wright-Patterson AFB, OH, Jan. and Feb. 1991.
- [11] Mercier, D. E. (1978) An extended Kalman filter for use in a shared aperture medium range tracker. MS thesis, AFIT/GE/ENG/78D-3, School of Engineering, Air Force Institute of Technology (AU), Wright-Patterson AFB, OH, Dec. 1978. Also DTIC Acc. No. ADA064191. (See also Maybeck, P. S., and Mercier, D. E. (1980) A target tracker using spatially distributed infrared measurements. *IEEE Transactions on Automatic Control*, **AC-25**, 2 (Apr. 1980), 222–225.)
- [12] Millner, P. P. (1982) Enhanced tracking of airborne targets using a correlator/Kalman filter. MS thesis, AFIT/GA/EE/82M, School of Engineering, Air Force Institute of Technology (AU), Wright-Patterson AFB, OH, Mar. 1982. Also DTIC Acc. No. ADA124884.
- [13] Muravez, R. J. (1989) Multiple model adaptive estimation and prediction with the harmonically balanced Kalman filter bank. MS thesis, California State Polytechnic University, Pomona, 1989.
- [14] Niblett, B. J. (1991) A multiple model adaptive estimator using first and second-order acceleration models for use in a forward-looking-infrared tracker. MS thesis, AFIT/GE/ENG/91J-03, School of Engineering, Air Force Institute of Technology (AU), Wright-Patterson AFB, OH, June 1991. Also DTIC Acc. No. ADA238799.
- [15] Rogers, S. K. (1981) Advanced tracking of airborne targets using forward looking infrared measurements. MS thesis, AFIT/GE/ENG/81D, School of Engineering, Air Force Institute of Technology (AU), Wright-Patterson AFB, OH, Dec. 1981. Also DTIC Acc. No. 115581. (See also Maybeck, P. S., and Rogers, S. K. (1983) Adaptive tracking of multiple hot-spot target IR images. *IEEE Transactions on Automatic Control*, **AC-28**, 10 (Oct. 1983), 937–943.)
- [16] Sheldon, S. N., and Maybeck, P. S. (1993) An optimizing design strategy for multiple model adaptive estimation and control. *IEEE Transactions on Automatic Control*, **38**, 4 (Apr. 1993), 651–654.
- [17] Stevens, R. D. (1989) Characterization of a reconfigurable multiple model adaptive controller using a STOL F-15 model. MS thesis, AFIT/GE/ENG/89D, School of Engineering, Air Force Institute of Technology (AU), Wright-Patterson AFB, OH, Dec. 1989. Also DTIC Acc. No. ADB139226. (See also Maybeck, P. S., and Stevens, R. D. (1991) Reconfigurable flight control via multiple model adaptive control methods. *IEEE Transactions on Aerospace and Electronic Systems*, **27**, 3 (May 1991), 470–480.)
- [18] Suizu, R. I. (1983) Advanced tracking of airborne targets using multiple model adaptive filtering techniques for adaptive field of view expansion. MS thesis, AFIT/GE/ENG/83D, School of Engineering, Air Force Institute of Technology (AU), Wright-Patterson AFB, OH, Dec. 1983. Also DTIC Acc. No. ADA141144. (See also Maybeck, P. S., and Suizu, R. I. (1985) Adaptive tracker field-of-view variation via multiple model filtering. *IEEE Transactions on Aerospace and Electronic Systems*, **AES-21**, 4 (July 1985), 529–539.)
- [19] The Analytic Sciences Corporation (1978) Advanced adaptive optics control techniques. Report TR-996-1 (prepared for the Air Force Weapons Laboratory, Kirtland AFB, NM), The Analytic Sciences Corporation, Reading, MA, Jan. 1978.
- [20] Tobin, D. M. (1986) A multiple model adaptive tracking algorithm for a high energy laser weapon system. MS thesis, AFIT/GE/ENG/86D-37, School of Engineering, Air Force Institute of Technology (AU), Wright-Patterson AFB, OH, Dec. 1986. Also DTIC Acc. No. ADA178978. (See also Tobin, D. M., and Maybeck, P. S. (1988) Enhancements to a multiple model adaptive estimator/image-tracker. *IEEE Transactions on Aerospace and Electronic Systems*, **24**, 4 (July 1988), 417–426.)

**Barbara J. Wheaton** was born in El Paso, TX. She received a B.S. in electrical engineering from the University of Texas at El Paso in 1985.

She entered the Air Force through the R.O.T.C. program at New Mexico State University in 1985. She worked as an engineer at the Central Inertial Guidance Test Facility at Holloman AFB, NM. In 1989 she entered the M.S.E.E. program at the Air Force Institute of Technology, and she was awarded that degree in June 1991. Currently, she is an aircraft subsystems engineer conducting operational test and evaluation at Edwards AFB, CA.

**Peter S. Maybeck** was born in New York, NY on February 9, 1947. He received the B.S. and Ph.D. degrees in aeronautical and astronautical engineering from M.I.T. in 1968 and 1972, respectively.

In 1968, he was employed by the Apollo Digital Autopilot Group of The C. S. Draper Laboratory, Cambridge, MA. From 1972 to 1973, he served as a military control engineer for the Air Force Flight Dynamics Laboratory and then joined the faculty of the Air Force Institute of Technology in June of 1973. He is currently Professor of Electrical Engineering, responsible for the graduate sequence in estimation and stochastic control and for individual advanced digital filtering and control courses. Current research interests concentrate on using optimal estimation techniques for guidance systems, tracking, adaptive systems and failure detection purposes.

Dr. Maybeck is author of numerous papers on applied optimal filtering as well as the book, *Stochastic Models, Estimation and Control* (Academic Press, Vol. 1—1979, Vols. 2 and 3—1982). He is a member of Tau Beta Pi, Sigma Gamma Tau, Eta Kappa Nu, and Sigma Xi. He was recipient of the DeFlorez Award (ingenuity and competence of research), the James Means Prize (excellence in systems engineering) and the Hertz Foundation Fellowship at M.I.T. in 1968. In all years from 1975 to 1993, he received commendation as outstanding Professor of Electrical Engineering at A.F.I.T. In December of 1978, he received an award from the Affiliate Societies Council of Dayton as one of the twelve outstanding scientists in Dayton, OH area. In March of 1980, he was presented with the Eta Kappa Nu Association's C. Holmes MacDonald Award, designating him as the outstanding electrical engineering professor in the United States under the age of 35 (he had placed second in this national competition for 1977 as well). In 1985, he received the Frederick Emmons Terman Award, the highest national award to a Professor of Electrical Engineering given by the American Society of Engineering Education. He is a Fellow of the I.E.E.E. and a member of the A.I.A.A., and he is the current I.E.E.E. Dayton Section Student Activities Chairman and a member of the I.E.E.E. Executive Committee of Dayton, and he previously served as Chairman of the local Automatic Control Group.

